DTU Library

A compact cyclic plasticity model with parameter evolution

Krenk, Steen; Tidemann, L.

Accepted Manuscript

A Compact Cyclic Plasticity Model with Parameter Evolution

S. Krenk, L. Tidemann

Please cite this article as: S. Krenk, L. Tidemann, A Compact Cyclic Plasticity Model with Parameter Evolution, *Mechanics of Materials* (2017), doi: 10.1016/j.mechmat.2017.07.012
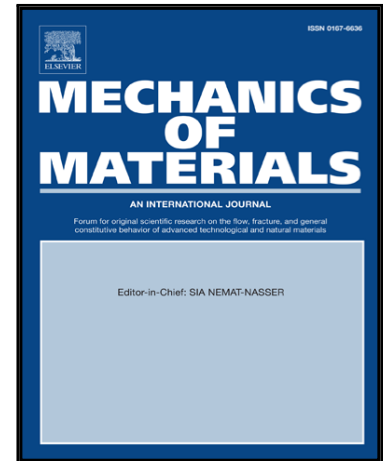
Highlights

- Cyclic plasticity model with five basic parameters via potentials and internal variables.

- Detailed development of plastic strain controlled by new shape parameter.

- An evolution format is presented for the five model parameters.

- Ability to accurately represent cyclic plasticity experiments is demonstrated.

A Compact Cyclic Plasticity Model with Parameter Evolution

S. Krenk[a)] and L. Tidemann[a,b)]

a) Department of Mechanical Engineering,
Technical University of Denmark,
DK-2800 Kongens Lyngby, Denmark

b) Facilities & Projects Discipline Area,
Mærsk Olie og Gas A/S,
DK-6700 Esbjerg, Denmark

Abstract

The paper presents a compact model for cyclic plasticity based on energy in terms of external and internal variables, and plastic yielding described by kinematic hardening and a flow potential with an additive term controlling the nonlinear cyclic hardening. The model is basically described by five parameters: external and internal stiffness, a yield stress and a limiting ultimate stress, and finally a parameter controlling the gradual development of plastic deformation. Calibration against numerous experimental results indicates that typically larger plastic strains develop than predicted by the Armstrong–Frederick model, contained as a special case of the present model for a particular choice of the shape parameter. In contrast to previous work, where shaping the stress-strain loops is derived from multiple internal stress states, this effect is here represented by a single parameter, and it is demonstrated that this simple formulation enables very accurate representation of experimental results. An extension of the theory to account for model parameter evolution effects, e.g. in the form of changing yield level, is included in the form of extended evolution equations for the model parameters. Finally, it is demonstrated that the model in combination with a simple parameter interpolation scheme enables representation of ratcheting effects.

Keywords: Cyclic plasticity; kinematic hardening; material degradation; model parameter evolution.

1. Introduction

A central feature of cyclic plasticity is the representation of the Bauschinger effect, in which the original elasto-plastic stress strain relation is stretched upon stress reversal, leading to nested loops, Masing (1927). Typically, full stress reversal leads to approximate doubling of the elastic stress range, suggesting representation in terms of a translating yield surface in the form of kinematic hardening, Prager (1956) and Ziegler (1959). The classic hardening rules do not lend themselves easily to the stretching of the stress-strain curve in the reversed yielding. This problem was resolved by Mroz (1967) by introducing a set of nested yield surfaces, each controlled by linear kinematic hardening. For circular/cylindrical yield surfaces this model is simple in principle, but it leads to a rather large number of parameters to keep track of all yield surfaces. For proportional loading the model leads to

stretched and nested loops, and there is a close analogy to the method of 'rainflow counting' used in fatigue life evaluation for irregular load histories.

An alternative to the multi-surface model is the two surface concept developed by Dafalias and Popov (1975, 1976) and Krieg (1975). In this concept the inner surface acts as a yield surface, while the relation to the bounding surface controls the hardening via translation of the yield surface. The hardening is derived using the relation between the current stress state on the yield surface and an equivalent point, characterized by a common direction of the normal on the bounding surface. When using a common homogeneous function for describing the yield surface as well as the bounding surface the intermediate steps can be eliminated, see e.g. Ottosen and Ristinmaa (2005). However, the model retains two variables, describing distances in stress space and varying in a discontinuous fashion.

A shift of focus from yield and bounding surfaces to a reference stress state within the yield surface was central in the model proposed by Armstrong and Frederick (1966). The key characteristic of the Armstrong–Frederick formulation based on the von Mises yield surface is the assumption of kinematic hardening, in which the center of the yield surface $\boldsymbol{\alpha}$ evolves according to a relation of the form

$$\dot{\boldsymbol{\alpha}} \, = \, c\left(\dot{\boldsymbol{\varepsilon}}_p - \frac{\dot{\varepsilon}_p^*}{\alpha_*}\boldsymbol{\alpha}\right), \tag{1}$$

where c is a characteristic parameter, $\dot{\boldsymbol{\varepsilon}}_p$ is the plastic strain rate, and the asterisk symbol indicates a normalized scalar form of the corresponding symbol. As the value of the center stress $\boldsymbol{\alpha}$ increases the rate of increase diminishes, eventually leading to asymptotic approach of the center stress $\boldsymbol{\alpha}$ to a limiting surface generated by the format of the model. A central point is that the bound in this model is on the internal stress state $\boldsymbol{\alpha}$, and not a tangent condition on the yield surface, thereby avoiding the construction of rules for the relative motion of two surfaces. This theory has been extended to several internal stress states, Chaboche and Rousselier (1983), and presented in terms of internal energy and flow potential by Chaboche (1986), and the thermodynamic consistency of multi-mechanism models was investigated by Wolff and Taleb (2008). Multi-surface, two-surface and Armstrong–Frederick models have been discussed in the extensive review by Chaboche (2008), also including visco-plastic models. An attractive feature of the Armstrong–Frederick type of model is the possibility of a fairly free selection of yield surfaces to account e.g. for anisotropy, Chun et al. (2002) or yield hinges in structural members, Tidemann and Krenk (2017).

One of the challenges of cyclic plasticity theories is the phenomenon of ratcheting, in which a non-zero mean stress leads to continuously increasing mean strain upon superposition of a cyclic stress component. The mean and cyclic components may be of the same type, e.g. uniaxial tension, or different components, e.g. axial and circumferential stresses in a tube. The modeling problem was considered by Ohno and Wang (1993a,b), who found that the lack of closure of the cycles in the original model by Armstrong and Frederick (1966) leads to excessive accumulated ratcheting strain. They proposed a modified model consisting of several internal stress states $\boldsymbol{\alpha}_j$, each bounded to a constant surface. This leads to a modification of the form of the basic Armstrong–Frederick evolution relation (1), changing the last term to a projection of the plastic strain rate tensor onto the tangent plane of the corresponding surface. It was subsequently demonstrated by Chaboche (1994), that the improved representation of ratcheting is mainly due to the non-linear representation of the second term in the evolution equation (1) following from the use of multiple

3

intervals, rather than from the projection property. Thus, a suitable non-linear form of the second term may be a key to an improved theory, as demonstrated in the present paper. An extensive series of experiments on ratcheting of metals were reported in Hassan and Kyriakides (1992), and Hassan et al. (1992). It was found that in order to model the ratcheting behavior the two-surface model of Dafalias and Popov (1975, 1976) needed a modification relating motion of the bounding surface to the development of plastic mean strain, while the model of Armstrong and Frederick (1966) needed a modification of the second term in (1) to a non-linear form. Alternatively, the performance of the Ohno-Wang model for ratcheting can be improved by supplementing the original kinematic hardening by combined kinematic-isotropic hardening, controlled by a balance parameter in each of the stress ranges, as proposed by Abdel-Karim (2010). An extensive overview of much of the previous work on cyclic plasticity was presented by Xiao et al. (2012), placing the theories within a general thermodynamic framework.

It is a common feature of cyclic behavior of metals that properties typically characterized by model parameters, such as elastic stiffness and yield stress, may change during the process. These effects may be included in a manner similar to traditional damage theory, see e.g. Lemaitre (1985) where both isotropic and kinematic hardening were introduced in the plasticity model and the evolution of the elastic stiffness was represented by continuous internal variables and coupled to the plastic evolution laws. As an alternative to the coupling between internal variables controlling model parameter evolution and plastic deformation, evolution of the model parameters can be introduced via a separate mechanism and a separate criterion, a so-called 2M2C model, where a damage strain is introduced similar to the plastic strain and has a separate evolution law, see e.g. Ibrahimbegovic et al. (2008). A detailed discussion of the relation between model parameters in relation to material characteristics was given by Pham et al. (2013), presenting relations integrating to an exponential development in terms of accumulated plastic strain.

In multi-axial deformation the cyclic hardening/softening will be highly influenced by non-proportionality of the strain path as discussed by Calloch and Marquis (1999) and Tarigopula et al. (2008). In multi-axial strain-controlled cycling the ratio of the amplitude of one strain component to the amplitude of another strain component, the so-called strain range ratio, has a large influence on the cyclic hardening/softening. In the case of bi-axial strain cycling with combined axial and shear cycling the phenomenon has been discussed by Benallal and Marquis (1987). The effect of non-proportionality may be accounted for in various ways e.g. a strain-path memory surface as discussed by Hopperstad et al. (1995).

The present paper develops a simple compact elasto-plastic model of Armstrong–Frederick type, in which the second term in the evolution equation for the center of the instantaneous yield surface is generalized to non-linear form by use of a single parameter that controls the development of the plastic strain. This non-linear form replaces the need for multiple additive internal stress states $\boldsymbol{\alpha}_j$. The result is a simple model with 5-parameters: yield stress and ultimate stress; external and internal elastic stiffness; and a non-dimensional parameter characterizing the development of the plastic strain. These can be read fairly directly off a typical experimental stress-strain curve. Each of the parameters can be given a development by an evolution equation relating model parameters with internal parameters. A basic form of the plasticity model is developed in section 2 from an internal energy potential, a yield function and a flow potential. The model characteristics are illustrated in section 3 and

4

the extension to include a non-linear representation of the gradual development of plasticity is introduced. The theory is extended to its full format including parameter evolution in section 4, where internal parameters are introduced to permit gradual changes of the yield stress, the ultimate stress, and the elastic and the elasto-plastic stiffness. The ability of the model to represent uniaxial cyclic experimental results is presented in section 5 for constant model parameters and the representation of cyclic hardening/softening by parameter evolution in section 6. Finally, the ability to represent ratcheting strain development by a parameter interpolation based on the load cycle characteristics is demonstrated in section 7.

2. Simple Cyclic Plasticity Model

In this section the basic theory of Armstrong–Frederick type cyclic elasto-plasticity is developed based on the concept of external and internal strains and their conjugate stresses. This 'minimum' cyclic plasticity model is then generalized to account for a more detailed description of the development of yielding in section 3 and of parameter evolution effects in section 4.

2.1. External and internal variables

The elastic properties are represented by a specific internal energy, given by the function $\varphi(\boldsymbol{\varepsilon}_e, \boldsymbol{\varepsilon}_i)$, where $\boldsymbol{\varepsilon}_e$ is the elastic strain, while $\boldsymbol{\varepsilon}_i$ is a set of internal strain parameters, that represent development of the internal state of the material. For a linear elastic material with a corresponding representation of the internal strain parameters the internal energy function is a quadratic form in the strain components:

$$\varphi(\boldsymbol{\varepsilon}_e, \boldsymbol{\varepsilon}_i) = \tfrac{1}{2}\boldsymbol{\varepsilon}_e^T \mathbb{C}_e\, \boldsymbol{\varepsilon}_e \,+\, \tfrac{1}{2}\boldsymbol{\varepsilon}_i^T \mathbb{C}_i\, \boldsymbol{\varepsilon}_i. \tag{2}$$

Here and in the following a notation is used that permits interpretation of stresses, strains and stiffness properties either as symmetric tensors or the equivalent 'vector–matrix' format. $\mathbb{C}_e$ is the symmetric elastic stiffness matrix, and $\mathbb{C}_i$ is an analogous symmetric internal stiffness matrix. The superscript T denotes transposition, securing consistency of the 'vector-matrix' notation.

The external observable stress $\boldsymbol{\sigma}$ corresponding to the elastic strain $\boldsymbol{\varepsilon}_e$ and an internal stress $\boldsymbol{\sigma}_i$ corresponding to the internal strain $\boldsymbol{\varepsilon}_i$ are obtained from the internal energy function via the derivatives

$$\boldsymbol{\sigma} \;= \partial_{\boldsymbol{\varepsilon}_e}\varphi \,= \mathbb{C}_e\, \boldsymbol{\varepsilon}_e\,, \tag{3}$$

$$\boldsymbol{\sigma}_i = \partial_{\boldsymbol{\varepsilon}_i}\varphi \,= \mathbb{C}_i\, \boldsymbol{\varepsilon}_i\,. \tag{4}$$

By convention the partial derivatives are in column format. The first of the relations reproduces the classic linear Hooke's law, while the second gives a similar linear relation between the internal stresses $\boldsymbol{\sigma}_i$ and the internal strains $\boldsymbol{\varepsilon}_i$.

2.2. Yield surface

The yield function $F(\boldsymbol{\sigma}, \boldsymbol{\sigma}_i)$ defines the yield surface bounding the elastic stress region,

$$F(\boldsymbol{\sigma}, \boldsymbol{\sigma}_i) \leq 0. \tag{5}$$

In the present model the yield function is of the form $F(\boldsymbol{\sigma} - \boldsymbol{\sigma}_i)$. This implies that the surface translates in stress space as prescribed by the internal stress $\boldsymbol{\sigma}_i$. The yield surface is given by

$$F(\boldsymbol{\sigma}, \boldsymbol{\sigma}_i) = \|\boldsymbol{\sigma} - \boldsymbol{\sigma}_i\| - \sigma_y, \tag{6}$$

where the symbol $\|\ \|$ denotes a norm of the multi-component stress state, and σ_y is the initial yield stress. In the following the norm will be taken as the von Mises equivalent stress $\sigma_e = \|\boldsymbol{\sigma}\|$, defined in terms of the deviatoric stress $\boldsymbol{\sigma}' = \boldsymbol{\sigma} - \frac{1}{3}\text{trace}(\boldsymbol{\sigma})$ by $\sigma_e^2 = \frac{3}{2}\sigma'_{\alpha\beta}\sigma'_{\alpha\beta}$.

2.3. Plastic flow

The plastic deformation is associated with the rate of energy dissipation, evaluated as the difference between the rate of energy supplied through the total strain rate $\dot{\boldsymbol{\varepsilon}}$ and the time derivative of the internal energy $\dot{\varphi}$,

$$\mathcal{D} = \boldsymbol{\sigma}^T \dot{\boldsymbol{\varepsilon}} - \dot{\varphi}(\boldsymbol{\sigma}, \boldsymbol{\sigma}_i) = \boldsymbol{\sigma}^T (\dot{\boldsymbol{\varepsilon}} - \dot{\boldsymbol{\varepsilon}}_e) - \boldsymbol{\sigma}_i^T \dot{\boldsymbol{\varepsilon}}_i \geq 0, \tag{7}$$

where the time derivative of the internal energy potential has been expressed by use of (3) and (4). This relation identifies the second factor in the first term as the plastic strain rate

$$\dot{\boldsymbol{\varepsilon}}_p = \dot{\boldsymbol{\varepsilon}} - \dot{\boldsymbol{\varepsilon}}_e, \tag{8}$$

corresponding to additive elastic and plastic strain rates.

The relations that govern the strain rates are defined by introducing a plastic flow potential $G(\boldsymbol{\sigma}, \boldsymbol{\sigma}_i)$, and assuming that the rate of dissipation $\mathcal{D}$ is maximized on an equipotential surface for given strain rates $\dot{\boldsymbol{\varepsilon}}_p, \dot{\boldsymbol{\varepsilon}}_i$. According to this principle the strain rates are proportional to the normal to the equipotential surface at the point $\boldsymbol{\sigma}, \boldsymbol{\sigma}_i$, corresponding to

$$\begin{aligned}
\dot{\boldsymbol{\varepsilon}} &= \dot{\boldsymbol{\varepsilon}}_e + \dot{\lambda}\,\partial_{\boldsymbol{\sigma}} G, \\
\mathbf{0} &= \dot{\boldsymbol{\varepsilon}}_i + \dot{\lambda}\,\partial_{\boldsymbol{\sigma}_i} G.
\end{aligned} \tag{9}$$

The common multiplier $\dot{\lambda}$ is determined by the consistency condition, securing that the stress state $\boldsymbol{\sigma}$ remains on the yield surface.

The flow potential contains the internal stress $\boldsymbol{\sigma}_i$ and its mathematical form is essential for controlling the motion of the yield surface in connection with cyclic plasticity. A simple plastic flow potential corresponding to the yield surface $F(\boldsymbol{\sigma}, \boldsymbol{\sigma}_i)$ in (6) can be expressed in the form

$$G(\boldsymbol{\sigma}, \boldsymbol{\sigma}_i) = F(\boldsymbol{\sigma}, \boldsymbol{\sigma}_i) + \frac{1}{2\sigma_m}\big(\|\boldsymbol{\sigma}_i\|^2 - \sigma_m^2\big), \tag{10}$$

where σ_m is a model parameter of dimension stress. The term σ_m^2 is included to make the limiting value of $G(\boldsymbol{\sigma}, \boldsymbol{\sigma}_i)$ equal to zero in analogy to the yield function, i.e. $F(\boldsymbol{\sigma}, \boldsymbol{\sigma}_i) = 0$ corresponds to maximum elastic capacity and $G(\boldsymbol{\sigma}, \boldsymbol{\sigma}_i) = 0$ corresponds to maximum plastic

capacity. It is an important feature of the flow potential format (10) that the yield function is of degree one in the stresses, while the additional hardening term is of higher degree in the internal stress $\boldsymbol{\sigma}_i$ - here two. This particular feature implies that increasing value of $\|\boldsymbol{\sigma}_i\|$ leads to faster growth of the second term, eventually stopping further increase at $\|\boldsymbol{\sigma}_i\| = \sigma_m$. This feature is discussed in detail in section 3 together with a simple generalization of of the hardening term.

Much of the present theory is retained for more general yield surfaces, if these are represented by a homogeneous function of degree one, thereby covering the cases of anisotropy via a modified von Mises yield surface, and yield hinges e.g. in structural members when using a yield surface format in the form of a sum of square roots of quadratic forms, Tidemann and Krenk (2017).

2.4. Elasto-plastic evolution equations

During elasto-plastic loading the stress $\boldsymbol{\sigma}$ remains on the yield surface, and thus the yield condition $F(\boldsymbol{\sigma}, \boldsymbol{\sigma}_i) = 0$ is identically satisfied during this time. The plastic multiplier is found by time differentiation of the yield function, followed by substitution of the stress rates $\dot{\boldsymbol{\sigma}}$ and $\dot{\boldsymbol{\sigma}}_i$ in terms of the equivalent strain rates $\dot{\boldsymbol{\varepsilon}}_e$ and $\dot{\boldsymbol{\varepsilon}}_i$ via (3) and (4). Finally, the strain rates are expressed by the flow rule (9), whereby the plastic multiplier is obtained as

$$\dot{\lambda} = \boldsymbol{\Gamma}^T \dot{\boldsymbol{\varepsilon}} \tag{11}$$

in terms of the one-dimensional array

$$\boldsymbol{\Gamma} = \frac{\mathbb{C}_e \left(\partial_{\boldsymbol{\sigma}} F\right)}{\left(\partial_{\boldsymbol{\sigma}} F\right)^T \mathbb{C}_e \left(\partial_{\boldsymbol{\sigma}} G\right) + \left(\partial_{\boldsymbol{\sigma}_i} F\right)^T \mathbb{C}_i \left(\partial_{\boldsymbol{\sigma}_i} G\right)}. \tag{12}$$

Plastic loading is based on the condition that the plastic multiplier $\dot{\lambda}$ calculated from this expression is positive. If this is not the case, the corresponding increment is elastic corresponding to $\dot{\lambda} = 0$.

The stress rate and internal stress rate now follow directly from the evolution equations (9) by multiplication with $\mathbb{C}_e$ and $\mathbb{C}_i$, respectively,

$$\begin{aligned}
\dot{\boldsymbol{\sigma}} &= \left[\mathbb{C}_e - \mathbb{C}_e \left(\partial_{\boldsymbol{\sigma}} G\right) \boldsymbol{\Gamma}^T\right] \dot{\boldsymbol{\varepsilon}}, \\
\dot{\boldsymbol{\sigma}}_i &= - \mathbb{C}_i \left(\partial_{\boldsymbol{\sigma}_i} G\right) \boldsymbol{\Gamma}^T \dot{\boldsymbol{\varepsilon}}.
\end{aligned} \tag{13}$$

These equations describe the evolution of stresses in response to an imposed strain history. The elastic part of the response follows by simply omitting the terms containing $\boldsymbol{\Gamma}$.

2.5. Relation to the Armstrong–Frederick model

The model of Armstrong and Frederick (1966) was developed for a von Mises material with kinematic hardening, governed by the evolution equation (1). It is of interest to compare this with the evolution equation for the internal stress $\boldsymbol{\sigma}_i$ in the basic form of the model developed above. When defining the stress norm by the equivalent stress, $\|\boldsymbol{\sigma}\|^2 = \sigma_e^2 = \frac{3}{2} \boldsymbol{\sigma}'^T \boldsymbol{\sigma}'$, the plastic strain rate follows from (9a) in the form

$$\dot{\boldsymbol{\varepsilon}}_p = \dot{\lambda} \partial_{\boldsymbol{\sigma}} G = \dot{\lambda} \frac{3}{2} \frac{\boldsymbol{\sigma}' - \boldsymbol{\sigma}_i'}{\|\boldsymbol{\sigma}' - \boldsymbol{\sigma}_i'\|}. \tag{14}$$

7

The corresponding scalar equivalent plastic strain rate is defined by $\dot{\varepsilon}_p^* = (\frac{2}{3}\dot{\boldsymbol{\varepsilon}}_p^T\dot{\boldsymbol{\varepsilon}}_p)^{1/2} = \dot{\lambda}$, and thus the plastic multiplier is defined by the equivalent plastic strain rate in the present case of the von Mises stress surface defined via the equivalent stress $\sigma_e = \sigma_y$.

The evolution of the internal stress $\boldsymbol{\sigma}_i$ then follows from (9b) by multiplication with the internal stiffness tensor $\mathbb{C}_i$ as

$$\dot{\boldsymbol{\sigma}}_i = -\mathbb{C}_i \dot{\lambda} \partial_{\boldsymbol{\sigma}_i} G = \mathbb{C}_i\Big(\dot{\lambda}\partial_{\boldsymbol{\sigma}} G - \frac{\dot{\lambda}}{2\sigma_m}\partial_{\boldsymbol{\sigma}_i}\|\boldsymbol{\sigma}_i\|^2\Big). \tag{15}$$

In this relation the first term is recognized as the plastic strain rate from (14), while the second term is evaluated by differentiation of the stress norm and identification of the plastic multiplier with the equivalent plastic strain rate. Hereby the evolution equation takes the form

$$\dot{\boldsymbol{\sigma}}_i = \mathbb{C}_i\Big(\dot{\boldsymbol{\varepsilon}}_p - \frac{3}{2}\frac{\dot{\varepsilon}_p^*}{\sigma_m}\boldsymbol{\sigma}_i'\Big). \tag{16}$$

The plastic strain rate $\dot{\boldsymbol{\varepsilon}}_p$ is deviatoric by (14), and for isotropic internal stiffness $\mathbb{C}_i$ the first factor degenerates to scalar stiffness, whereby the Armstrong–Frederick evolution format (1) is recovered from the basic form of the present model. It is seen that the effect of the internal stress term in the evolution equation is easily modified by changing the second term in the definition of the flow potential as discussed in the following section.

3. Model Characteristics and Enhanced Flow Potential

In this section the cyclic elasto-plastic model developed above is specialized to uniaxial format and the basic features and their relation to the model parameters are identified. The specific features of the transition from elastic to mainly plastic behavior is then used to develop a compact but more general representation of the flow potential, containing one additional parameter.

3.1. Uniaxial relations

In the uniaxial model the internal energy is given in terms of the strain ε_e and the internal strain ε_i as

$$\varphi(\varepsilon_e, \varepsilon_i) = \tfrac{1}{2}\varepsilon_e^T E_e\,\varepsilon_e + \tfrac{1}{2}\varepsilon_i^T E_i\,\varepsilon_i. \tag{17}$$

This expression contains two material parameters: the elastic modulus E_e and the internal elastic modulus E_i. The uniaxial yield function takes the form

$$F(\sigma, \sigma_i) = |\sigma - \sigma_i| - \sigma_y, \tag{18}$$

where $|\ |$ denotes the absolute value, and σ_y is the uniaxial yield stress. Finally, the corresponding uniaxial flow potential is

$$G(\sigma, \sigma_i) = F(\sigma, \sigma_i) + \frac{1}{2\sigma_m}\big(|\sigma_i|^2 - \sigma_m^2\big). \tag{19}$$

The stress parameter σ_m represents a hardening limit as demonstrated below.

In total the model contains four parameters E_e, E_i, σ_y and σ_m. Of these the two first relate directly to the stiffness, while the two latter describe characteristic stress levels. This direct interpretation is illustrated below, and turns out to establish a fairly direct correspondence between each parameter and a characteristic feature of the stress-strain curve.

3.2. Uniaxial evolution equations

The evolution equations of the model follow from evaluation of the derivatives of the yield function $F(\sigma, \sigma_i)$ and the flow potential $G(\sigma, \sigma_i)$ with respect to the stress σ and internal stress σ_i. The evolution equations contain the factor Γ from (12) consisting of two terms. The first term, describing the elastic contribution, is

$$(\partial_\sigma F)^T \, \mathbb{C}_e \, (\partial_\sigma G) \; = \; E_e. \tag{20}$$

Each of the derivatives with respect to the stress σ contain the factor $\text{sign}(\sigma - \sigma_i) = \partial_\sigma |\sigma - \sigma_i|$ describing the direction of the loading process, but as this factor appears twice the effect cancels, and the factor does not appear explicitly in this term. The second term in the denominator, involving the internal variables, defines the plastic hardening modulus

$$H \; = \; (\partial_{\sigma_i} F)^T \, \mathbb{C}_i \, (\partial_{\sigma_i} G) \; = \; E_i \Big[1 \, - \, \text{sign}(\sigma - \sigma_i) \frac{\sigma_i}{\sigma_m} \Big]. \tag{21}$$

Here the contribution E_i is similar to (20), while the second contribution combines the sign-function from the derivative of F with the normalized internal stress σ_i/σ_m from the derivative of G.

Evolution equations for both the stress σ and the internal stress σ_i follow from substitution of the uniaxial expressions (20) and (21) into the two general evolution equations (13),

$$\dot{\sigma} \; = \; \dot{\sigma}_i \; = \; \frac{\dot{\varepsilon}}{1/E_e \, + \, 1/H}. \tag{22}$$

A direct interpretation of the hardening modulus H is obtained by writing the stress relation in the form

$$\dot{\varepsilon} = \frac{\dot{\sigma}}{E_e} + \frac{\dot{\sigma}}{H} \; = \; \dot{\varepsilon}_e \, + \, \dot{\varepsilon}_p \,. \tag{23}$$

This relation clearly defines $1/H$ as an additional plastic flexibility. It follows immediately that the elastic case is described by an infinite value of H.
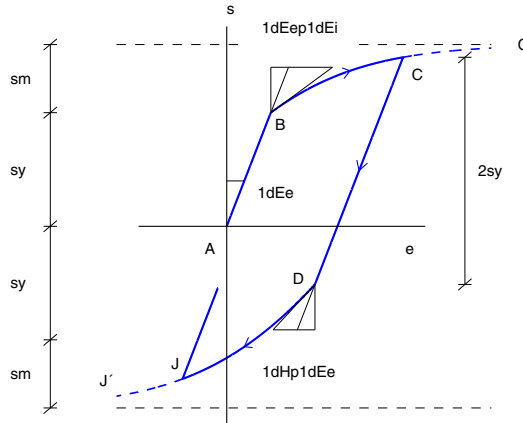

Figure 1: Stress-strain curve of simple model with simple translation term.

9

The role of $1/H$ as an additional plastic flexibility makes a further analysis of the expression (21) important for identification of the role of the individual model parameters. In Fig. 1 the first part AB of the initial loading curve with $\sigma < \sigma_y$ is elastic with stiffness modulus E_e. When entering the plastic regime for the first time at $\sigma = \sigma_y$ the stiffness changes. At this point the internal stress σ_i is still at its initial value $\sigma_i = 0$, and thus $H = E_i$ at B. With increasing straining the internal stress σ_i increases until $H = 0$, which is reached in the limit $\sigma_i = \sigma_m$. Thus, the monotonic ultimate stress limit is defined by

$$\sigma_u \,=\, \sigma_m \,+\, \sigma_y\,. \tag{24}$$

This defines the model parameter σ_m as the stress by which the ultimate stress σ_u exceeds the initial yield stress σ_y.

In the figure unloading is initiated at C, leading to an elastic part CD with stress range $2\sigma_y$ and flexibility $1/E_e$. At D elasto-plastic behavior starts, and the flexibility increases to $1/E_e + 1/H$. The internal stress σ_i, representing the center of the yield surface, does not change during the elastic unloading along CD. The expression (21) can therefore be used to express the sum of the hardening modulus at C and at D as

$$H_D \,+\, H_C \,=\, 2E_i\,. \tag{25}$$

Along BC the hardening modulus has decreased from E_i towards the asymptotic value zero. If the plastic straining is large compared to the elastic yield strain σ_y/E_e, then $H_C \ll E_i$ and thus $H_D \simeq 2E_i$. This corresponds to the plastic strain developing at about half the rate at D as compared to the initial plastic straining at B. This generates the often observed cyclic elasto-plastic behavior, that the first loading branch of the stress-strain curve appears as stretched by a factor of two in the following cyclic branches. This behavior is illustrated by the examples in section 5.

3.3. Enhanced flow potential

The theory developed above constitutes a minimal, but quite versatile, cyclic plasticity model – essentially the Armstrong–Frederick theory, when using the von Mises yield surface. There are only four model parameters: the elastic stiffness E_e, the internal stiffness E_i and the yield and ultimate stress levels σ_y and $\sigma_u = \sigma_y + \sigma_m$. The model represents the principal features of cyclic plasticity well. However, the transition from onset of plastic straining e.g. at the points B or D in Fig. 1 to fully developed plasticity at C' or J' is described by only two parameters: the initial slope, defined by the elasto-plastic flexibility $1/E_e + 1/H$, and the ultimate asymptotic stress limit $\pm\sigma_u$. The transition is governed by the plastic hardening modulus H, given by (21). It consists of a constant E_i, defining the flexibility at initiation of plastic deformation, minus a term that is linear in the internal stress σ_i. As illustrated in the examples in section 5 an improved quantitative representation of experimental results for steel can be obtained, if the linear term is modified to exhibit a slower than linear increase with respect to σ_i.

In the modified model the gradient of the flow potential with respect to the internal stress is expressed in the form

$$\partial_{\sigma_i} G \,=\, -\,\mathrm{sign}(\sigma - \sigma_i) \,+\, \frac{\sigma_i}{(1-\alpha)\sigma_m + \alpha|\sigma_i|}\,, \qquad \alpha < 1\,. \tag{26}$$
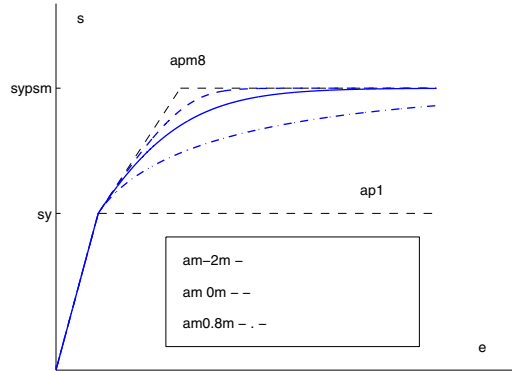
10

Figure 2: Influence of parameter α on stress-strain curve.

In the limit $\alpha = 0$ the previous basic model is recovered, while the upper limit $\alpha < 1$ is necessary to retain the last term as an increasing function of σ_i. The flow potential $G(\sigma, \sigma_i)$ follows from integration of (26), whereby

$$G = F + \frac{1}{\alpha}\Big\{ |\sigma_i| - \sigma_m - \frac{1 - \alpha}{\alpha}\sigma_m \ln\Big(1 + \alpha\frac{|\sigma_i| - \sigma_m}{\sigma_m}\Big)\Big\}, \quad \alpha < 1. \tag{27}$$

It is seen that $G \to 0$ when approaching the ultimate stress limit, where $|\sigma_i| \to \sigma_m$. Furthermore, it is easily verified by expansion of the logarithm that the original flow potential (19) is recovered in the limit $\alpha = 0$.

The hardening modulus follows as

$$H = (\partial_{\sigma_i} F)\, \mathbb{C}_i\, (\partial_{\sigma_i} G) = E_i\Big[1 - \text{sign}(\sigma - \sigma_i)\frac{\sigma_i}{(1 - \alpha)\sigma_m + \alpha|\sigma_i|}\Big]. \tag{28}$$

The ultimate stress limit σ_u corresponds to $H = 0$. The particular parametrization used in the generalized form (28) leads to the same role of the parameter σ_m in the relation (24) giving the ultimate stress for σ_u as the sum of the yield stress σ_y and the stress σ_m. With a parametrization that retains the role of σ_m in defining the ultimate stress level, the role of the non-dimensional parameter α is simply to modify the transition curve between initiation of plastic straining and fully developed plasticity as illustrated in Fig. 2. It is seen that a negative value of the parameter α delays the development of plastic strain, concentrating the curve more into the corner formed by the intersection of the constant hardening part of the stress-strain curve and the curve marking the ultimate stress level. However, as illustrated by the experimental data in section 5 typical values of α for steel are positive, with $\alpha \simeq 0.8$ as fairly representative and shown in Fig. 2.

4. Full Model with Parameter Evolution

In this section the full multi-dimensional plasticity model is developed and supplemented by a systematic framework for parameter evolution. The characteristics and increased flexibility of the enhanced flow potential (27) are easily extended to multi-dimensional formats

by replacing the absolute values $|\sigma - \sigma_i|$ and $|\sigma_i|$ by the norms $\|\boldsymbol{\sigma} - \boldsymbol{\sigma}_i\|$ and $\|\boldsymbol{\sigma}_i\|$. The derivatives will not be the sign-function but normalized vectors analogous to a multi-dimensional sign-function.

In uniaxial as well as multi-axial cyclic plasticity it is often found, e.g. Hassan and Kyriakides (1992) and Chun et al. (2002), that cyclic plasticity leads to hardening or softening in the form of an increase or decrease of the apparent ultimate stress $\sigma_u = \sigma_y + \sigma_m$. In analogy with the change of the characteristic internal stress state $\boldsymbol{\sigma}_i$ the ultimate stress was represented by Chun et al. (2002) in terms of the accumulated equivalent plastic strain ε_p as

$$\sigma_u = \sigma_u^0 + K\big(1 - \mathrm{e}^{-N\varepsilon_p}\big). \tag{29}$$

In this formula σ_u^0 is the initial value of the ultimate stress, and the asymptotic value after large plastic straining then is $\sigma_u^\infty = \sigma_u^0 + K$. A direct formulation in terms of (29) would introduce the accumulated plastic strain ε_p as an independent variable of the theory. A more universal form in terms of an evolution equation for σ_u is obtained by differentiation of the relation (29) with respect to time, leading to

$$\dot{\sigma}_u = \dot{\lambda} N(\sigma_u^\infty - \sigma_u), \tag{30}$$

where σ_u is the current value of the ultimate stress, and the relation $\dot{\lambda} = \dot{\varepsilon}_p$ has been used. The evolution equation (30) has the same format as that of the internal variable $\boldsymbol{\varepsilon}_i$ in (9b), illustrating that evolution of the parameters of the model can be treated in a similar way as the internal variables. An extension of the plasticity model developed above to full multidimensional form including evolution of the model parameters is outlined in the following.

4.1. Theory with model parameter evolution

Evolution of the model parameters can be included in a manner similar to traditional damage theory. It is done by introducing an extra set of internal variables in the energy formulation in the form of strain-like evolution parameters $\boldsymbol{\xi}$. To permit evolution of the stiffness the stiffness matrices are considered as functions of $\boldsymbol{\xi}$, and a separate term is added to the internal energy,

$$\varphi(\boldsymbol{\varepsilon}_e, \boldsymbol{\varepsilon}_i, \boldsymbol{\xi}) = \tfrac{1}{2}\boldsymbol{\varepsilon}_e^T \mathbb{C}_e(\boldsymbol{\xi})\boldsymbol{\varepsilon}_e + \tfrac{1}{2}\boldsymbol{\varepsilon}_i^T \mathbb{C}_i(\boldsymbol{\xi})\boldsymbol{\varepsilon}_i + \varphi_d(\boldsymbol{\xi}), \tag{31}$$

where $\varphi_d(\boldsymbol{\xi})$ is a function to be specified to get an appropriate evolution of the model parameters. The energy-conjugate stress and stress-like parameters are defined by

$$\boldsymbol{\sigma} = \partial_{\boldsymbol{\varepsilon}_e}\varphi = \mathbb{C}_e(\boldsymbol{\xi})\boldsymbol{\varepsilon}_e, \tag{32}$$

$$\boldsymbol{\sigma}_i = \partial_{\boldsymbol{\varepsilon}_i}\varphi = \mathbb{C}_i(\boldsymbol{\xi})\boldsymbol{\varepsilon}_i, \tag{33}$$

$$\boldsymbol{\eta} = \partial_{\boldsymbol{\xi}}\varphi, \tag{34}$$

where $\boldsymbol{\eta}$ are stress-like evolution parameters, conjugate to $\boldsymbol{\xi}$.

It is assumed that evolution of the model parameters only occurs during plastic loading, and thus the model parameter evolution criterion coincides with the yield surface. Evolution of the yield surface is introduced in the yield function via the yield stress in the form

$$F(\boldsymbol{\sigma}, \boldsymbol{\sigma}_i, \boldsymbol{\eta}) = \|\boldsymbol{\sigma} - \boldsymbol{\sigma}_i\| - \sigma_y(\boldsymbol{\eta}). \tag{35}$$

12

This formulation enables evolution of the yield stress in a form similar to traditional isotropic hardening/softening.

The evolution of the model parameters is governed by the plastic flow potential, which has to be modified as well. It is desirable to enable evolution of all five model parameters – E_e, E_i representing stiffness, σ_y, σ_m representing stress levels, and α representing the gradual development of plastic straining. The flow potential including evolution of the model parameters is defined as

$$G = F + \frac{1}{\alpha}\Big\{ \|\boldsymbol{\sigma}_i\| - \sigma_m - \frac{1-\alpha}{\alpha}\,\sigma_m \ln\Big(1 + \alpha\frac{\|\boldsymbol{\sigma}_i\| - \sigma_m}{\sigma_m}\Big)\Big\} + G_{ei}(\boldsymbol{\eta}), \tag{36}$$

where $\sigma_y = \sigma_y(\boldsymbol{\eta})$, $\sigma_m = \sigma_m(\boldsymbol{\eta})$ and $\alpha = \alpha(\boldsymbol{\eta})$. The term $G_{ei}(\boldsymbol{\eta})$ is introduced to enable evolution parameters related to the stiffness parameters to be separated from the remaining evolution parameters.

The evolution equations relating the evolution of stress and stress-like parameters to a strain increment are determined following the same procedure as in section 2. They are conveniently expressed with two system stiffness matrices, that include stiffness related to elastic strains and strain-like evolution parameters, and stiffness related to elastic strains, internal strains and strain-like evolution parameters, respectively. These total stiffness matrices are defined as

$$\mathbb{C}_{ed}^T = \begin{bmatrix} \mathbb{C}_e(\boldsymbol{\xi}) & \mathbf{0} & \partial_{\boldsymbol{\xi}}^T\boldsymbol{\sigma} \end{bmatrix}, \tag{37}$$

$$\mathbb{C}_{eid} = \begin{bmatrix} \mathbb{C}_e(\boldsymbol{\xi}) & \mathbf{0} & \partial_{\boldsymbol{\xi}}^T\boldsymbol{\sigma} \\ \mathbf{0} & \mathbb{C}_i(\boldsymbol{\xi}) & \partial_{\boldsymbol{\xi}}^T\boldsymbol{\sigma}_i \\ (\partial_{\boldsymbol{\xi}}^T\boldsymbol{\sigma})^T & (\partial_{\boldsymbol{\xi}}^T\boldsymbol{\sigma}_i)^T & \partial_{\boldsymbol{\xi}}^T\boldsymbol{\eta} \end{bmatrix}. \tag{38}$$

Furthermore the total gradients of the yield surface and the plastic flow potential $\boldsymbol{\partial}F$ and $\boldsymbol{\partial}G$ are defined as

$$\boldsymbol{\partial}F = [\,\partial_{\boldsymbol{\sigma}}^T F\,,\, \partial_{\boldsymbol{\sigma}_i}^T F\,,\, \partial_{\boldsymbol{\eta}}^T F\,]^T, \tag{39}$$

$$\boldsymbol{\partial}G = [\,\partial_{\boldsymbol{\sigma}}^T G\,,\, \partial_{\boldsymbol{\sigma}_i}^T G\,,\, \partial_{\boldsymbol{\eta}}^T G\,]^T. \tag{40}$$

The plastic multiplier is given in terms of these quantities as

$$\dot{\lambda} = \frac{(\boldsymbol{\partial}F)^T\,\mathbb{C}_{ed}}{(\boldsymbol{\partial}F)^T\,\mathbb{C}_{eid}\,(\boldsymbol{\partial}G)}\,\dot{\boldsymbol{\varepsilon}}, \tag{41}$$

and the increment of the different stress and stress-like parameters then follows as

$$\begin{bmatrix} \dot{\boldsymbol{\sigma}} \\ \dot{\boldsymbol{\sigma}}_i \\ \dot{\boldsymbol{\eta}} \end{bmatrix} = \Big(\mathbb{C}_{ed} - \frac{\mathbb{C}_{eid}\,(\boldsymbol{\partial}G)\,(\boldsymbol{\partial}F)^T\,\mathbb{C}_{ed}}{(\boldsymbol{\partial}F)^T\,\mathbb{C}_{eid}\,(\boldsymbol{\partial}G)}\Big)\,\dot{\boldsymbol{\varepsilon}}. \tag{42}$$

It is noted that if evolution of the model parameters is not introduced in the evolution equations, the general relation (42) reduces to the classic plasticity format (13).

13

4.2. Model parameter evolution

Model parameter evolution has been incorporated into the theory via a scaling factor on the stiffness matrices $\mathbb{C}_e$ and $\mathbb{C}_i$, and on the parameters σ_y, σ_m and α. In relation to the present theory the five primary variables are $\boldsymbol{\xi} = [\xi_e, \xi_i, \xi_{\sigma_y}, \xi_{\sigma_m}, \xi_\alpha]$ with energy conjugates $\boldsymbol{\eta} = [\eta_e, \eta_i, \eta_{\sigma_y}, \eta_{\sigma_m}, \eta_\alpha]$. In the present formulation the effects of these evolution parameters are considered independent, and they are introduced into the theory in a form that generalizes the exponential format described by (29) and (30).

The three parameters η_{σ_y}, η_{σ_m} and η_α are introduced as scaling factors of the form

$$\sigma_y = \eta_{\sigma_y}\sigma_y^0, \qquad \sigma_m = \eta_{\sigma_m}\sigma_m^0, \qquad \alpha = \eta_\alpha\alpha^0, \tag{43}$$

where the superscript 0 refers to the initial value. The format of the model for each of the scaling factors η_{σ_y}, η_{σ_m} and η_α are identical, and will be described by the generic symbol η without subscript. The scaling factor η is energy conjugate to the internal variable ξ, with a relation here taken in the following exponential form

$$\eta = \frac{\partial \varphi}{\partial \xi} = \eta^\infty - (\eta^\infty - \eta^0)\mathrm{e}^{-\xi/\xi^*}. \tag{44}$$

The parameters η^0 and η^∞ denote the initial value of the scaling factor and its limiting value after infinite plastic deformation. The parameter ξ^* describes the scaling of the evolution process. It follows from integration that this relation is obtained when a term

$$\varphi_d(\xi) = \eta^\infty\xi + (\eta^\infty - \eta^0)\xi^*\mathrm{e}^{-\xi/\xi^*} \tag{45}$$

is added to the internal potential for each of the three parameters σ_y, σ_m and α. The internal parameter ξ only develops during yielding and evolves similar to the flow rule (9b), whereby

$$\dot{\eta} = \frac{\partial \eta}{\partial \xi}\dot{\xi} = -\frac{\partial \eta}{\partial \xi}\frac{\partial G}{\partial \eta}\dot{\lambda}. \tag{46}$$

When evaluating the derivative $\partial\eta/\partial\xi$ from the exponential relation (44) the evolution equation for the scaling factor η takes the form

$$\dot{\eta} = -\dot{\lambda}\,\frac{\eta^\infty - \eta}{\xi^*}\frac{\partial G}{\partial \eta}. \tag{47}$$

For the yield stress $\partial G/\partial\eta = -\sigma_y^0$, and the scaling factor η_{σ_y} becomes an exponential function of λ, representing the accumulated plastic strain. For the scaling parameters η_{σ_m} and η_α the derivative of the potential G is non-trivial and the evolution of these parameters thereby less direct. In the actual numerical implementation the scaling factors η_{σ_y}, η_{σ_m} and η_α follow from the evolution equations (42).

In the case of stiffness evolution the parameters ξ_e and ξ_i modify the magnitude of the corresponding stiffness matrices $\mathbb{C}_e$ and $\mathbb{C}_i$ directly as

$$\mathbb{C}_e = \tilde{\eta}_e(\xi_e)\mathbb{C}_e^0 = \left[\tilde{\eta}_e^\infty - (\tilde{\eta}_e^\infty - \tilde{\eta}_e^0)\mathrm{e}^{-\xi_e/\xi_e^*}\right]\mathbb{C}_e^0 \tag{48}$$

14

with a similar relation for $\mathbb{C}_i(\xi_i)$. In these expressions $\tilde{\eta}_e$ and $\tilde{\eta}_i$ are scaling parameters, but not conjugate to the parameters ξ_e and ξ_i. The evolution of the scaling factors $\tilde{\eta}_e$ and $\tilde{\eta}_i$ follow evolution relations similar to (46), e.g.

$$\dot{\tilde{\eta}}_e = \frac{\partial \tilde{\eta}_e}{\partial \xi_e} \dot{\xi}_e = -\frac{\partial \tilde{\eta}_e}{\partial \xi_e} \frac{\partial G}{\partial \eta_e} \dot{\lambda} . \tag{49}$$

The derivative $\partial G/\partial \eta_e$ makes use of the conjugate variable η_e. A simple choice is therefore to introduce the stiffness evolution via the extra term

$$G_{ei}(\eta_e, \eta_i) = -\eta_e - \eta_i \tag{50}$$

in the flow potential (36), thereby reducing the G-derivatives in (49) to $\partial G/\partial \eta_e = \partial G/\partial \eta_i = -1$. The evolution equations (42) give the increments of the conjugate variables η_e and η_i, and it is a simple matter to recalculate the current values to corresponding values of the scaling factors $\tilde{\eta}_e$ and $\tilde{\eta}_i$ and the associated internal variables ξ_e and ξ_i.

Here, the parameter evolution has been based on the exponential format (44) and (48), and as illustrated in the following examples this fits experimental data quite well. However, the procedure used here to introduce the basic evolution format can also be modified to represent the evolution via power functions or rational functions of the internal variables $\boldsymbol{\xi}$.

5. Characteristics of the Uniaxial Model

In this section the uniaxial characteristics of the present model for elasto-plasticity without parameter evolution are identified, and the performance of the model on a number of published cyclic tests from literature is illustrated together with results from alternative models used for representation of these test results.

5.1. Calibration

It is often useful to evaluate the backbone curve of a cyclic loading history when calibrating cyclic plasticity models. The backbone curve can typically be used for the initial estimation of model parameters and the calibration can be finalized with use of the full
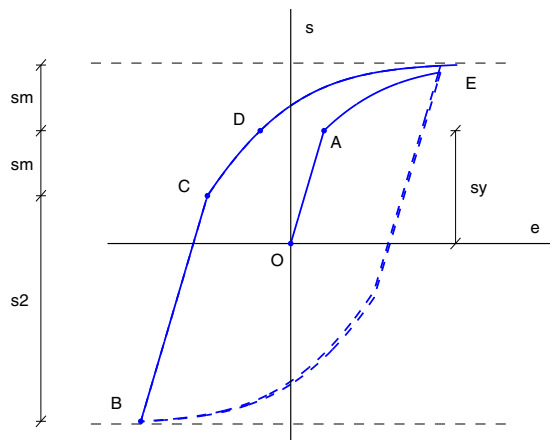

Figure 3: Conceptual calibration procedure.

15

Table 1: Calibration procedure.

1. Determine	E_e	by	$E_e = (\sigma_C - \sigma_B)/(\varepsilon_C - \varepsilon_B)$.
2. Determine	σ_y	by	$\sigma_y = (\sigma_C - \sigma_B)/2$.
3. Determine	E_i	by	secant stiffness at CD and E_e
		or	tangent stiffness at C or D and E_e.
4. Determine	σ_m	by	$\sigma_m \simeq |\sigma_B| - \sigma_y$
		or	$\sigma_m \simeq |\sigma_E| - \sigma_y$
		or	$\sigma_m \simeq (\sigma_E - \sigma_B)/2 - \sigma_y$.
5. Determine	α	by	the shape of the curve DE.

cyclic response. In the present case all the model parameters can be observed fairly directly from the backbone curve. The conceptual backbone curve of the model is highlighted as a part of the full response in Fig. 3.

In Fig. 3 the point O is the initial stress free state, A corresponds to the first state of yielding, B is the initial stress state at reloading, C is the point where plastic loading starts again, D is the point where the center of the yield surface passes Origo, corresponding to a stress state of $\sigma = \sigma_y$, and E is the point where loading ends. The stress-strain relationship is linear-elastic from B to C with a change in stress between these two states of $2\sigma_y$. From the point C to the point D the stress-strain relation is almost linear, corresponding to constant hardening when σ_i approaches Origo. This linear relation is almost independent of α. From the point D to the point E the stress-strain relationship is non-linear with a clear dependence on α. This type of backbone curve with a linear-elastic, a nearly constant hardening and a non-linear hardening part is observed for many materials.

A direct calibration procedure is described in Table 1. It has been used for different test specimens, described in the following examples, to show the characteristics of the model. The calibrated model parameters are shown in Table 2. It is seen that the parameter α lies in the interval 0.68–0.95, with a typical value of 0.80. As seen from Fig. 2 this corresponds to faster development of plastic strain than in the Armstrong–Frederick model.

Table 2: Model parameters.

Figure	E_e [GPa]	E_i/E_e	σ_y [MPa]	σ_m/σ_y	α
4, 5	195	1.3	190	1.92	0.88
6	200	1.5	150	2.30	0.94
7(a)	65	3.2	150	1.67	0.82
7(b)	90	2.0	150	1.33	0.68
8	220	4.0	40	8.25	0.95
9	170	2.0	360	1.72	0.82

16

5.2. Symmetric cycling

The calibration procedure described above is used for different test samples with symmetric cycling, Shi et al. (2012). Two different scenarios of strain-controlled symmetric cycling are considered; in the first case the mean strain is zero and the strain amplitude is initially 1% and then increases by 0.5% for each cycle. In the second case the mean strain is 1% and the amplitude is initially 0.5% and increases 0.5% for each cycle. The test results are shown in Fig. 4 together with the results from the present model with parameters given in Table 2. It is observed that except for the first cycle, the shape of the hysteresis loops as well as the stress levels are predicted accurately by the model. The zero mean strain cycling is predicted slightly more accurately than the non-zero mean strain cycling. This relates to the symmetric format of the model; the zero mean strain cycling is perfectly symmetric whereas the non-zero mean strain cycling is not perfectly symmetric with respect to the strain. A more accurate representation of the first cycle can be obtained by introducing an appropriate evolution function that only affects the first part of the plastic straining, using the framework described in section 4.
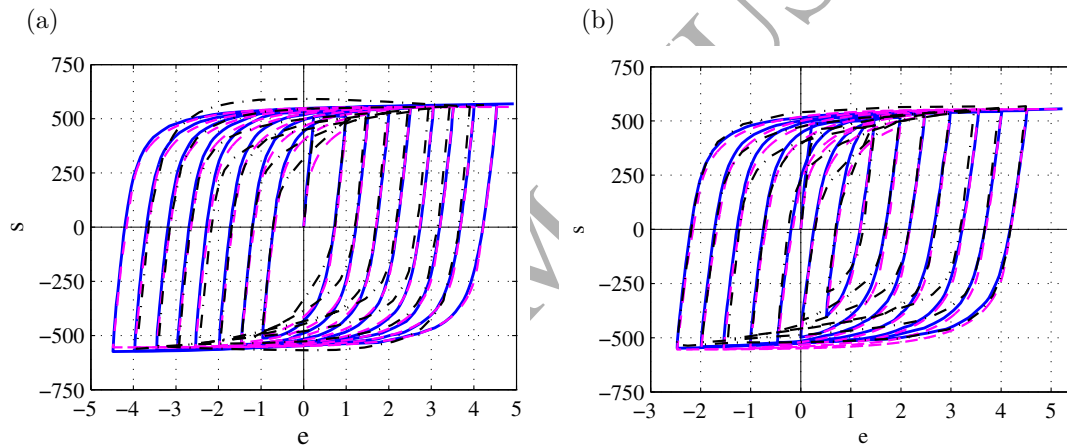

Figure 4: Symmetric cycling: Shi et al. (2012) experiment (——), model (— · —). Present model (– –).

Figure 4 also shows results from the model proposed by Shi et al. (2012) based on a combination of a peak based model and a backbone curve divided into two separate parts, an elastic part and a hardening part. The hardening part is approximated by curve fitting and the separation point between the elastic and the plastic part is given by the strain. It is observed from Fig. 4 that despite the simplicity of the present model, it gives a more accurate representation of the experimental data.

5.3. Non-symmetric cycling

The present model can also represent non-symmetric cycling fairly accurately as illustrated by the strain-controlled experiment shown in Fig. 5. The strain is cycled between a positive maximum strain which is initially 1% increasing by 0.5% for each cycle, and a negative minimum strain of -1%.
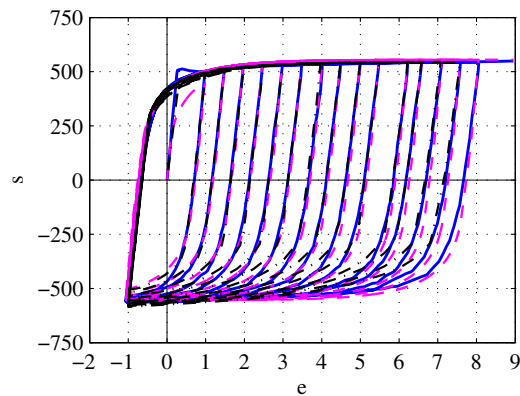
Figure 5: Non-symmetric cycling: Shi et al. (2012) experiment (—), model (– · –). Present model (– –).

With the exception of the first few cycles the shapes of the hysteresis loops as well as the stress levels are predicted quite accurately. As previously noted, the representation of the first cycle can be improved by use of an appropriate evolution of the model parameters.

5.4. Comparison with other models

Popov and Petersson (1978) investigated cyclic plasticity in thin tubular specimens experimentally and used a multi-surface type material model. This was combined with different hardening parameters with formulations based on the plastic strain. The experimental results along with the model proposed by Popov and Petersson (1978) and the present model are shown in Fig. 6. It is seen that the present model reproduces both the stress levels and the shape of the hysteresis loops quite well.
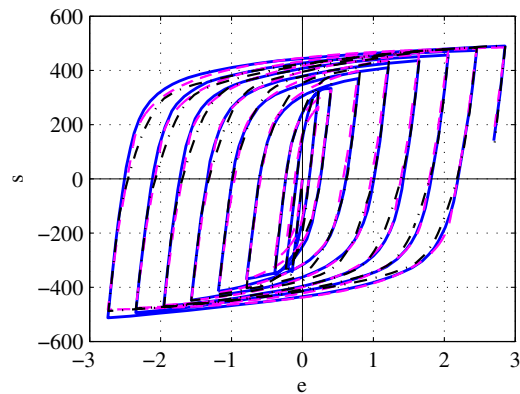

Figure 6: Popov and Petersson (1978) experiment (—), model (– · –). Present model (– –).

Several models have been based on the model proposed by Armstrong and Frederick (1966) and the subsequent modifications made by Chaboche (1989) and Ohno and Wang (1993a,b). One focus area has been visco-plastic models, and recently Guo et al. (2013) developed a model for particle-reinforced metal matrix composites and alloys. In this model
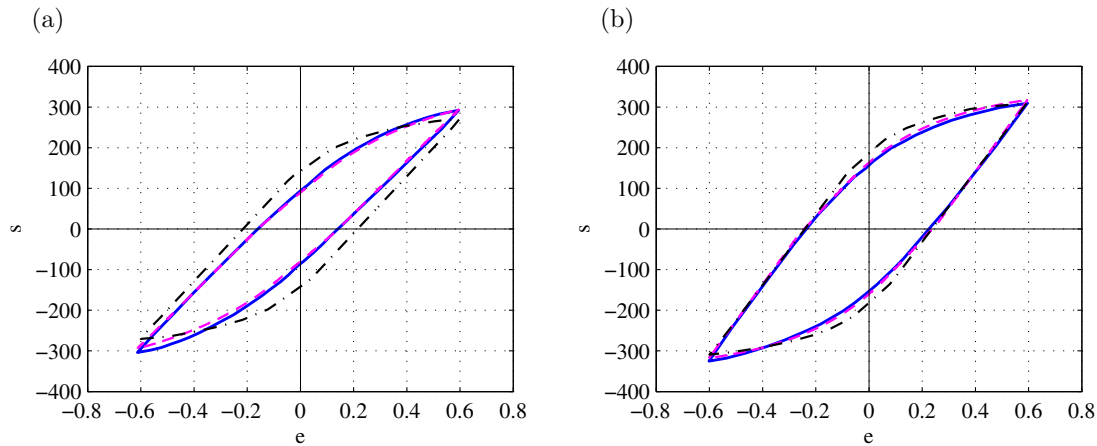
18

Figure 7: Guo et al. (2013) experiment (——), model (– · –). Present model (– –). (a) Matrix, (b) alloy.

the matrix material and the particle reinforcement have individual material parameters and the resulting material parameters of the alloy are found via a combination depending on the volume fraction of the particle reinforcement. The present model can also be used for such a type of problems if calibrated properly. Figure 7 shows experimental stabilized response together with theoretical results from Guo et al. (2013) as well as results from the present model, calibrated separately for the two tests with parameters given in Table 2 for matrix material alone and for a composite with 14% reinforcement particles. The ability to capture the shape of the stress-strain curves is notable, and the parameters from Table 2 may be related to the representation of mixture properties.

A visco-plastic model with focus on cyclic hardening/softening was developed by Kang et al. (2003), based on Ohno and Wang (1993a,b). This model typically requires a fairly large number of parameters, and it is of interest to compare its representation of individual cycles with that of the present model, with the five parameters shown in Table 2. Figure 8 shows a comparison between experimental data, the model proposed by Kang et al. (2003),
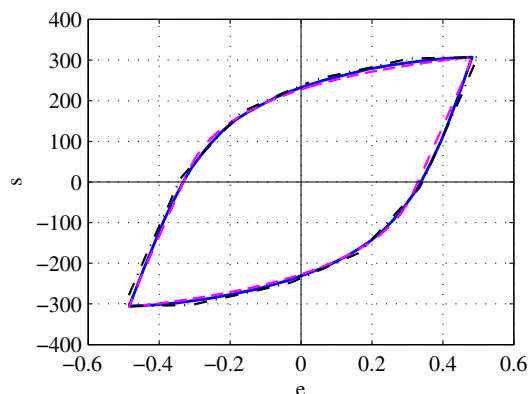

Figure 8: Kang et al. (2003) experiment (——), model (– · –). Present model (– –).

19

and the present calibrated model. It is observed that both models are rather accurate in representing the shape and the stress levels of the hysteresis loop, but the present model with only five model parameters.

There are also other types of models, e.g. the so-called 2M1C models (2 Mechanisms, 1 Criterion) models. Such a model has been proposed by Velay et al. (2006) in relation to hot working tool steel. An example of a comparison between the 2M1C model and the present model is shown in Fig. 9 for a case in which the viscous effect on the plastic response is negligible. Both models are predicting the shape of the hysteresis loop and the stress levels rather well, the present being the more accurate.
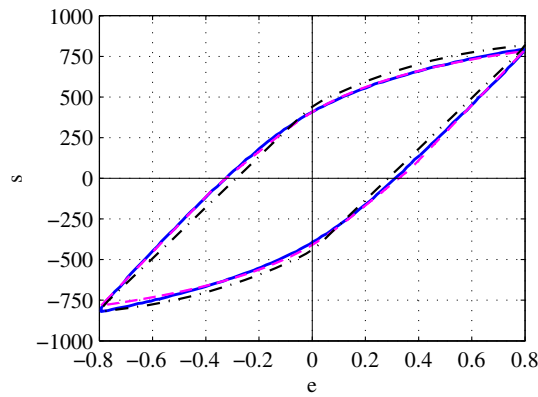

Figure 9: Velay et al. (2006) experiment (—), model $(- \cdot -)$. Present model $(- -)$.

6. Cyclic Hardening/Softening by Parameter Evolution

This section presents three examples illustrating parameter evolution. The initial model parameters are shown in Table 3 which is comparable to Table 2. The initial value of the scaling parameters is $\eta^0 = 1$ and the parameters defining the evolution of the initial parameters are shown in Table 4.

6.1. Softening and hardening for constant amplitude strain cycling

A case of cyclic softening, i.e. degradation, is observed for carbon steel CS1020 as reported by Hassan and Kyriakides (1992). With a set of relatively simple evolution functions

Table 3: Model initial parameters.

Figure	E_e^0 [GPa]	E_i^0/E_e^0	σ_y^0 [MPa]	σ_m^0/σ_y^0	α^0
10	187	4.5	200	1.75	0.08
11	185	2.5	100	2.10	0.10
12(b)	200	3.5	140	0.68	0.45

Table 4: Model evolution parameters.

Figure	ξ_e^* [–]	ξ_i^* [–]	$\xi_{\sigma_y}^*$ [MPa]	$\xi_{\sigma_m}^*$ [MPa]	ξ_α^* [kPa]	$\tilde{\eta}_e^\infty$	$\tilde{\eta}_i^\infty$	$\eta_{\sigma_y}^\infty$	$\eta_{\sigma_m}^\infty$	η_α^∞
10	2.0	0.7	20	-	2.0	0.0	0.0	0.55	1	11.75
11	9.0	1.0	100	50	1.8	0.0	0.4	0.00	2.62	9.20
12(b)	7.0	0.9	10	10	1.0	0.0	0.0	0.64	4.42	1.98

the uniaxial behaviour can be represented rather accurately with the present model as il-lustrated in Fig. 10. The experiment is strain controlled and the test specimen is cycled between 1% and -1% strain.
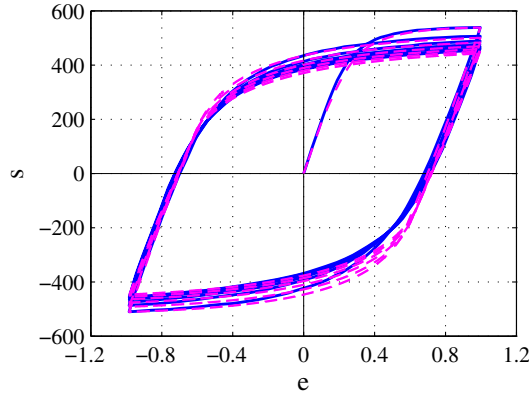

Figure 10: Degradation: Hassan and Kyriakides (1992) experiment (——). Present model (– –).

It is observed in Fig. 10 that the combined evolution mechanisms reproduce the shape of the hysteresis loops, the characteristic stress levels and the change in shape from the first loading branch to the remaining loading branches. There is a small discrepancy between the experimental results and the modelled results in the lower right corner, but overall the modelled and the experimental results are very similar.

The theory including model parameter evolution described in section 4 can also be used to model cyclic hardening. Hassan and Kyriakides (1992) showed results of stainless steel with an initial significant cyclic hardening. In the experiments the hardening is primarily of the ultimate capacity, while the yield limit remains fairly constant. This corresponds to increasing σ_m with asymptotic stabilisation ($\eta_{\sigma_m}^\infty = 2.62$) and relatively slow change of σ_y ($\xi_{\sigma_y}^* \gg \xi_{\sigma_m}^*$). The experimental results are shown in Fig. 11 together with the modelled results. The experiment is strain controlled, and cycled between 2.0% and -2.0% strain.

As shown in Fig. 11 the present model is fairly accurate for this type of behaviour as well. Each hysteresis cycle is represented rather accurately and the characteristic stress levels are also well represented by the model.
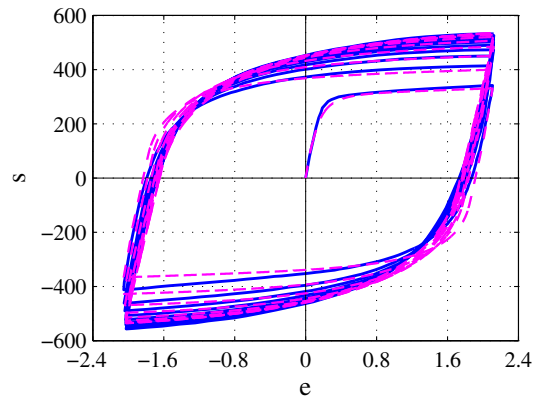
21

Figure 11: Degradation: Hassan and Kyriakides (1992) experiment (——). Present model (– –).

6.2. Hardening for increasing strain cycles

Similarly Kang et al. (2003) made experiments on cyclic hardening materials with a strain controlled experiment. The cycling was symmetric about zero mean strain, but with increasing amplitude starting at 0.18% and increasing with 0.30% for each cycle. The experimental results along with the results modelled by Kang et al. (2003) are shown in Fig. 12(a) whereas the experimental results together with results from the present model are shown in Fig. 12(b).

It is observed in Fig. 12 that the present model performs quite well - now with a total of 15 model parameters, five for the initial elasto-plastic model and 10 for the parameter evolution. The present model reproduces the hysteresis loops and the characteristic stress levels quite well, even with the very simple parameter evolution functions.
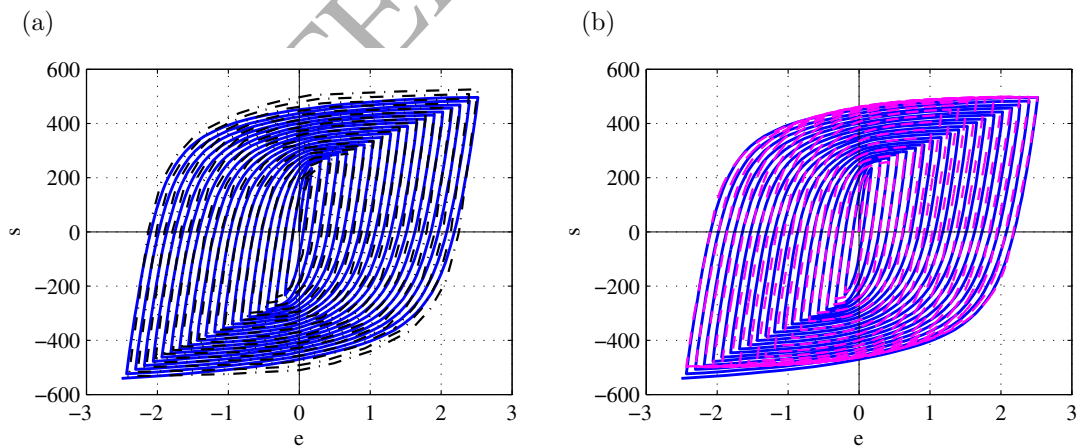
(a)   (b)

Figure 12: Cyclic hardening: (a) Kang et al. (2003) experiment (——), model (– · –). (b) Kang et al. (2003) experiment (——). Present model (– –).

22

7. Biaxial Ratcheting

To illustrate the capability to model multi-axial loading and ratcheting, experiments presented by Ohno and Wang (1993b) are modelled. In three experiments a specimen is loaded to a constant tension stress state σ giving an initial axial strain ε, and subsequently the shear strain γ is cyclically varied between $\pm\Delta\gamma/2$ resulting in axial strain ratcheting. The values used in the experiments are given in Table 7. In the biaxial stress state the elastic and the internal stiffness matrices take the form

$$\mathbb{C}_e = \left[\begin{array}{cc} E_e & 0 \\ 0 & \mu_e \end{array} \right], \quad \mathbb{C}_i = \left[\begin{array}{cc} E_i & 0 \\ 0 & \mu_i \end{array} \right] \tag{51}$$

where E_e is the elastic Young's modulus and μ_e is the elastic shear modulus, whereas E_i and μ_i are the corresponding internal stiffness parameters. The initial model parameters are listed in Table 5. While the ratio E_i/E_e is similar to previous examples these hold no equivalent of the present ratio μ_i/μ_e.

In the experiments there is no direct cycling of the axial stress, but rather an indirect effect due to the interaction with the cycling of the shear stain. The combined effect of the different levels of prestress, strain range and degrees of non-proportionality can be represented via a change in the single parameter σ_m as given by an interpolation scheme introduced by Benallal and Marquis (1987),

$$\eta_{\sigma_m}^\infty(\Lambda) = \Lambda\, \eta_{\sigma_m}^\infty(1) + (1 - \Lambda)\, \eta_{\sigma_m}^\infty(0), \quad \Lambda = 1 - \cos^2\theta, \tag{52}$$

where θ is the angle between the incremental plastic strain $d\boldsymbol{\varepsilon}^p$ and the incremental deviatoric stress $d\boldsymbol{\sigma}'$, formally considered as vectors. In practice the interpolation does not cover the interval $0 \leq \Lambda \leq 1$, but a typically much smaller interval between two experiments used as the basis of the interpolation. The value of Λ as well as the parameter $\eta_{\sigma_m}^\infty(\Lambda)$ in these two cases are used as basis, and the interpolated value of $\eta_{\sigma_m}^\infty$ is then obtained by estimating a representative value of Λ for each of the remaining experiments. In the experiments the parameter σ_m increases whereby $\eta_{\sigma_m}^\infty > 0$. It turns out that the corresponding attenuation parameter $\xi_{\sigma_m}^*$ can be assumed proportional to the relative increase of σ_m whereby the ratio $(\eta_{\sigma_m}^\infty - 1)/\xi_{\sigma_m}^*$ is a constant, that is determined from the uniaxial hysteresis curve. The resulting evolution parameters are listed in Table 7. The experiments marked with ∇ and $\times$ in Table 6 were used as basis for determining the values at the end of the interpolation interval. The remaining values of $\eta_{\sigma_m}^\infty$ are then obtained by the interpolation procedure. It is noted that only the parameter σ_m^∞ has been subjected to interpolation to account for different values of Λ. In practical cases with unknown stress states at different times and different points in a structure an initial analysis may be performed to determine a representative value for Λ for the given loading condition and subsequently the analysis may be performed with values determined from the interpolation scheme.

Table 5: Biaxial ratcheting: Model initial parameters.

E_e [GPa]	μ_e [GPa]	E_i/E_e	μ_i/μ_e	σ_y^0 [MPa]	σ_m^0/σ_y^0	α^0
162	60.9	2.8	74.5	180	1.72	0.08

Table 6: Biaxial ratcheting: Experiment characteristics.

Marker	σ [MPa]	$\Delta\gamma/\sqrt{3}$ [%]	$\Lambda \cdot 10^3$
$\triangledown$	100	0.8	8.84
$\times$	50	1.0	1.37
$\circ$	50	0.8	2.24
$\bullet$	50	0.6	4.10

Table 7: Biaxial ratcheting: Model evolution parameters.

η_α^∞	ξ_α^* [kPa]	$\eta_{\sigma_m}^\infty$	$\dfrac{\eta_{\sigma_m}^\infty - 1}{\xi_{\sigma_m}^*}$ [GPa^{-1}]
10.6	2.5	1.43 ($\triangledown$) 2.10 ($\times$)	86.4

The uniaxial stress-strain behaviour is shown in Fig. 13 with all four model parameter combinations and they all show good correspondence with the experimental behaviour and are indistinguishable from one another in the uniaxial single-cycle.
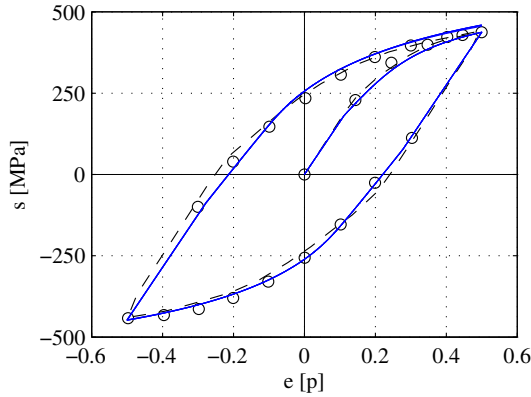

Figure 13: Uniaxial cycling. Tanaka et al. (1991) experiment ($\circ$). Ohno and Wang (1993b) model ($--$). Present model (—).

The biaxial ratcheting effect is shown in Fig. 14 where the accumulated axial strain is plotted against the number of shear strain cycles. The modelled results agree well with the experimental results as illustrated in Fig. 14. There is a slight offset between the modelled results and the experimental results when $\sigma = 50\,\text{MPa}$ and $\Delta\gamma/\sqrt{3} = 1.0\,\%$ in the cycles 10–15, but the difference is almost negligible.

8. Conclusions

A simple five-parameter model has been developed for cyclic plasticity. The model parameters are the external and internal stiffness, the yield stress and a stress range parameter
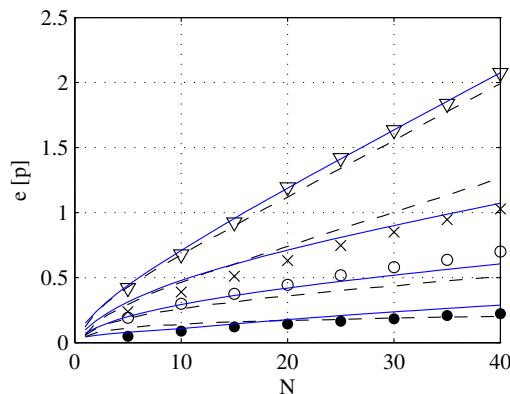
Figure 14: Biaxial cycling. Tanaka et al. (1991) experiment ($\triangledown$,$\times$,$\circ$,$\bullet$). Ohno and Wang (1993b) model ($-\,-$). Present model (—).

σ_m representing the difference between ultimate stress and the yield stress, and finally a non-dimensional shape parameter α describing the development of plastic strain. Each of the five parameters describe a fairly well defined independent feature of the stress strain relation, and thus the parameters can be estimated initially as independent, and subjected to subsequent minor adjustment, if necessary. In the present format the shape parameter α, replaces the often used representation of the internal stress $\boldsymbol{\sigma}_i$ as a sum of stress states, each with their own parameters. The present single parameter modification permits an accurate representation of the cyclic stress-strain loops, and the parameter α exhibits a fairly modest variation for the experimental data analyzed. It also accounts for the experimental observation that the developed plastic strains are larger than predicted by the classic Armstrong–Frederick model, contained in the present model as the special case $\alpha = 0$.

The five-parameter plasticity formulation has been extended by including possible evolution of the model parameters in a format similar to traditional damage-theory. The format contains the plastic multiplier, and evolution of the model parameters can therefore be included by a fairly direct extension of the plasticity format. The ability of this formulation to describe cyclic hardening and softening has been demonstrated by comparison with fairly extensive uniaxial experimental data. The model has also been used for two-dimensional ratcheting, representing the effect of the range magnitude and component ratio via a parameter interpolation scheme involving only the stress range parameter σ_m.

In the literature various forms of the Armstrong–Frederick plasticity model have been recast into visco-plastic form by replacing the plastic strain rate term in the evolution equation of the internal stresses $\boldsymbol{\sigma}_i$ with an expression in terms of current stress. As this transformation does not influence the format of the second term, the present format of this term can be retained in a visco-plastic formulation of the model. However, this aspect has not been included in the present paper.

Acknowledgements

References

References

Abdel-Karim, M., 2010. An extension for the Ohno–Wang kinematic hardening rules to incorporate isotropic hardening. International Journal of Pressure Vessels and Piping 87, 170–176.

Armstrong, P. J., Frederick, C. O., 1966. A mathematical representation of the multiaxial Bauschinger effect. Tech. Rep. Report RD/B/N731, CEGB, Central Electricity Generating Board, Berkeley, UK, (Reprinted in Materials at High Tempertures, 24, 1–26, 2007).

Benallal, A., Marquis, D., 1987. Constitutive equations for nonproportional cyclic elasto-viscoplasticity. Journal of Engineering Materials and Technology ASME 109, 326–336.

Calloch, S., Marquis, D., 1999. Triaxial tension-compression tests for multiaxial cyclic plasticity. International Journal of Plasticity 15, 521–549.

Chaboche, J. L., 1986. Time-independent constitutive theories for cyclic plasticity. International Journal of Plasticity 2, 149–188.

Chaboche, J. L., 1989. Constitutive equations for cyclic plasticity and cyclic viscoplasticity. International Journal of Plasticity 5, 247–302.

Chaboche, J. L., 1994. Modeling of ratchetting: evaluation of various approaches. European Journal of Mechanics and Solids 13, 501–518.

Chaboche, J. L., 2008. A review of some plasticity and viscoplasticity constitutive theories. International Journal of Plasticity 24, 1642–1693.

Chaboche, J. L., Rousselier, G., 1983. On the plastic and viscoplastic constitutive equations – Part 1: Rules developed with internal variable concept. Journal of Pressure Vessel Technology 105, 153–158.

Chun, B. K., Jinn, J. T., Lee, J. K., 2002. Modeling the Bauschinger effect for sheet metals, Part I: Theory. International Journal of Plasticity 18, 571–595.

Dafalias, Y. F., Popov, E. P., 1975. A model of nonlinearly hardening materials for complex loading. Acta Mechanica 21, 173–192.

Dafalias, Y. F., Popov, E. P., 1976. Plastic internal variables formalism of cyclic plasticity. Journal of Applied Mechanics 43, 645–651.

Guo, S., Kang, G. Z., Zhang, J., 2013. A cyclic visco-plastic constitutive model for time-dependent ratchetting of particle-reinforced metal matrix composites. International Journal of Plasticity 40, 101–125.

Hassan, T., Corona, E., Kyriakides, S., 1992. Ratcheting in cyclic plasticity, Part II: Multi-axial behavior. International Journal of Plasticity 8, 117–146.

26

Hassan, T., Kyriakides, S., 1992. Ratcheting in cyclic plasticity, Part I: Uniaxial behavior. International Journal of Plasticity 8, 91–116.

Hopperstad, O. S., Langseth, M., Remseth, S., 1995. Cyclic stress-strain behaviour of alloy AA6060 T4, Part II: Biaxial experiments and modelling. International Journal of Plasticity 11, 741–762.

Ibrahimbegovic, A., Jehel, P., Davenne, L., 2008. Coupled damage-plasticity constitutive model and direct stress interpolation. Computational Mechanics 42, 1–11.

Kang, G. Z., Ohno, N., Nebu, A., 2003. Constitutive modeling of strain range dependent cyclic hardening. International Journal of Plasticity 19, 1801–1819.

Krieg, R. D., 1975. A practical two surface plasticity theory. Journal of Applied Mechanics 42, 641–646.

Lemaitre, J., 1985. Coupled elasto-plasticity and damage constitutive equations. Computer Methods in Applied Mechanics and Engineering 51, 31–49.

Masing, G., 1927. Wissenschaftliche Veröffentlichungen aus dem Siemens-Konzern. Band III.

Mroz, Z., 1967. On the description of anisotropic workhardening. Journal of the Mechanics and Physics of Solids 15, 163–175.

Ohno, N., Wang, J.-D., 1993a. Kinematic hardening rules with critical state of dynamic recovery, Part I: Formulation and basic features for ratchetting behavior. International Journal of Plasticity 9, 375–390.

Ohno, N., Wang, J.-D., 1993b. Kinematic hardening rules with critical state of dynamic recovery, Part II: Application to experiments of ratchetting behavior. International Journal of Plasticity 9, 391–403.

Ottosen, N. S., Ristinmaa, M., 2005. The Mechanics of Constitutive Modeling. Elsevier, Amsterdam, The Netherlands.

Pham, M. S., Holdsworth, S. R., Janssens, K. G. F., Mazza, E., 2013. Cyclic deformation response of AISI 316L at room temperature: Mechanical behaviur, microstructural evolution, physically-based evolutionary constitutive modelling. International Journal of Plasticity 47, 143–164.

Popov, E. P., Petersson, H., 1978. Cyclic metal plasticity: Experiments and theory. Journal of the Engineering Mechanics Division, ASCE. 114, EM6, 1371–1388.

Prager, W., 1956. A new method of analyzing stresses and strains in work-hardening plastic solids. Journal of Applied Mechanics 23, 493–496.

Shi, G., Wang, M., Bai, Y., Wang, F., Shi, Y., Wang, Y., 2012. Experimental and modeling study of high-strength structural steel under cyclic loading. Engineering Structures 37, 1–13.

27

Tanaka, E., Murakami, S., Mizuno, M., Yamada, H., Iwata, K., 1991. Inelastic behavior of modified 9Cr-1Mo steel and its unified constitutive model. In: Proceedings of the 6th International Conference on Mechanical Behaviour of Materials, Vol. 3. Pergamon Press, Oxford.

Tarigopula, V., Hopperstad, O., Langseth, M., Clausen, A. H., 2008. Elastic-plastic behaviour of dual-phase, high-strength steel under strain-path changes. European Journal of Mechanics and Solids 27, 764–782.

Tidemann, L., Krenk, S., 2017. Cyclic plastic hinges with degradation effects for frame structures. Journal of Engineering Mechanics, (accepted for publication).

Velay, V., Bernhart, G., Penazzi, L., 2006. Cyclic behavior modeling of a tempered martensitic hot work tool steel. International Journal of Plasticity 22, 459–496.

Wolff, M., Taleb, L., 2008. Consistency for two multi-mechanism models in isothermal plasticity. International Journal of Plasticity 24, 2059–2083.

Xiao, Y., Chen, J., Cao, J., 2012. A generalized thermodynamic approach for modeling nonlinear hardening behaviors. International Journal of Plasticity 38, 102–122.

Ziegler, H., 1959. A modification of Prager's hardening rule. Quarterly of Applied Mathematics 17, 55–65.